Simultaneous Estimation of T_1, T_2 and B_1 Maps From Relaxometry MR Sequences

Fang Cao, Olivier Commowick, Elise Bannier, Christian Barillot

VisAGeS U746 INSERM/INRIA, IRISA UMR CNRS 6074, Rennes, France

Abstract. Interest in quantitative MRI and relaxometry imaging is rapidly increasing to enable the discovery of new MRI disease imaging biomarkers. While DESPOT1 is a robust method for rapid whole-brain voxel-wise mapping of the longitudinal relaxation time (T_1), the approach is inherently sensitive to inaccuracies in the transmitted flip angles, defined by the B_1 inhomogeneity field, which become more severe at high field strengths (e.g., 3T). We propose a new approach for simultaneously mapping the B_1 field, M_0 (proton density), T_1 and T_2 relaxation times based on regular fast T_1 and T_2 relaxometry sequences. The new method is based on the intrinsic correlation between the T_1 and T_2 relaxometry sequences to jointly estimate all maps. It requires no additional sequence for the B_1 correction. We evaluated our proposed algorithm on simulated and in-vivo data at 3T, demonstrating its improved accuracy with respect to regular separate estimation methods.

1 Introduction

Quantitative MRI is becoming more and more important to study the brain micro-structure and to provide calibrated measures of brain tissue properties from MRI that are crucial to obtain MR imaging biomarkers. The gold standard methods for longitudinal and transverse relaxation times (T_1 and T_2) mappings require long acquisition times that are often not applicable for clinical use. Many methods have been proposed to speed up the scanning procedures.

The driven-equilibrium single-pulse observation of T_1 (DESPOT1) [4] and the Carr-Purcell-Meiboom-Gill (CPMG) multi-echo sequence for measuring T_2 [7] have gained significant popularity over the past decades due to their superior time efficiency, allowing fast T_1 and T_2 mapping with high resolution and large spatial coverage. However, both DESPOT1 and CPMG methods suffer from a strong dependence on an accurate knowledge of the Flip Angle (FA), which leads to significant errors in the presence of the non uniform radiofrequency excitation field B_1 [2]. This is particularly problematic at high field strengths, where B_1 variations can be over 20% and in situ FA correction is necessary [2, 5]. It is therefore commonly accepted that DESPOT1 and CPMG at 3T or higher field strengths need to be combined with an appropriate B_1 correction method [10, 9], especially for T_1 estimation [3]. Different prospective methods have been presented to compensate for B_1 inhomogeneities by acquiring additional or new sequences. Parker et al. proposed a methodology for estimating T_1 using a two-point technique with a standard multislice gradient echo

sequence [10]. Treier compensated B_1 field inhomogeneities in T_1 mapping by performing an additional measurement using an optimized fast B_1 mapping technique [15]. Deoni presented a method that combines the DESPOT1 data with at least one inversion-prepared SPGR data to obtain an unique solution for the B_1 map [3]. Dowell et al. proposed a B_1 mapping sequence using spoiled gradient echo (SPGR) and 180° signal null [5]. Yarnykh developed a fast B_1 mapping sequence that consists of two identical RF pulses followed by two delays of different durations [17].

However, since B_1 map acquisition takes up precious scanning time and most retrospective studies do not include B_1 field mapping sequences, we wish to keep the data acquisition protocol of DESPOT1 and CPMG multi-echo sequences. We therefore introduce a new combined algorithm to estimate T_1 and T_2 relaxation times, and B_1 inhomogeneities without requiring additional B_1 acquisitions. The estimation of all maps is formulated as an energy minimization problem on the whole image without any prior knowledge of the inner structure of the subject.

In Sect. 2, we review the regular estimation methods and propose our new algorithm for joint estimation with B_1 correction. We validate our method using synthetic phantom and in vivo data sets in Sect. 3. The experimental results are given in Sect. 4 to demonstrate the effectiveness of the proposed method.

2 Methods

2.1 Regular T_1 and T_2 Estimation

Following the DESPOT1 algorithm [4], traditional T_1 estimation uses two SPGR sequences. The MR signals measured at two flip angles α_i are modeled as

$$I^{\dagger}_{\alpha_i}(T_1, M_{0,T_1}) = \frac{M_{0,T_1}(1-\exp(-\mathrm{TR}/T_1))\sin\alpha_i}{1-\exp(-\mathrm{TR}/T_1)\cos\alpha_i},\ i=1,2 \tag{1}$$

where T_1 is the longitudinal relaxation time, M_{0,T_1} is proportional to the proton density M_0 and TR is the repetition time. T_1 and M_{0,T_1} are optimized through a least squares problem to fit $I^{\dagger}_{\alpha_i}(T_1, M_{0,T_1})$ to the observed signals S_{α_i}. Such a problem has an analytical solution for M_{0,T_1} and T_1 [4]. Then, the traditional T_2 estimation is performed by minimizing $\sum_{j=1}^{n}(S_{\mathrm{TE}_j} - I^{\dagger}_{\mathrm{TE}_j})^2$ [14] where S_{TE_j} ($j=1,\ldots,n$, n being the echo train length) are the acquired signals measured at TE_j, the j-th echo time in the CPMG sequence, and $I^{\dagger}_{\mathrm{TE}_j}$ is the corresponding simulated signal of the j-th echo. We use the Extended Phase Graph (EPG) algorithm [7, 9] to model the simulated signals. This algorithm tracks the multiple coherence pathways of spins after consecutive periods that model precession, relaxation and refocusing, and has been used to calculate the echo decay curves in CPMG sequence yielding precise monoexponential T_2 quantification [9, 12, 8]. Rather than computing the time evolution of magnetization vectors, the EPG algorithm uses the magnetization phase state vector $\boldsymbol{F} = [F_1, F_1^*, Z_1, F_2, F_2^*, Z_2, \cdots, F_n, F_n^*, Z_n]^T$ to describe the spin system at a given time. The states F and F^* refer to the dephasing and rephasing of the

spins in the transverse plane. The states Z refer to the spins along the longitudinal axis that maintain their phase. For the j-th echo, $\boldsymbol{F}_j$ is calculated by

$$\boldsymbol{F}_j = \boldsymbol{E}(T_1, T_2)\boldsymbol{T}\boldsymbol{R}_j(\alpha)\boldsymbol{E}(T_1, T_2)\boldsymbol{F}_{j-1},\ j = 1, \cdots, n \tag{2}$$

where $\boldsymbol{F}_0$ is proportional to the proton density M_0. The matrix $\boldsymbol{R}_j$ represents the effects of RF refocusing, depending on the nominal flip angle α of the refocusing pulse for each echo train. The matrix $\boldsymbol{E}$ represents T_1 and T_2 relaxation between successive echoes. The matrix $\boldsymbol{T}$ represents the phase transitions for each echo train. The amplitude $I^{\dagger}_{\mathrm{TE}_j}$ of the j-th echo is given by the first element of $\boldsymbol{F}_j$. More details on the EPG algorithm can be found in [9, 12, 8].

2.2 Simultaneous Relaxation Times and B_1 Field Estimation

The traditional DESPOT1 algorithm and T_2 relaxometry estimation provide a solution for T_1, T_2 and M_0 estimation. However, this solution lacks accuracy in the presence of inhomogeneities in the B_1 transmission field. In this study, we use a combined model of DESPOT1 and EPG algorithms to estimate T_1, T_2, M_0 and B_1 simultaneously. This joint model, thanks to the intrinsic dependence between the T_1 and T_2 relaxometry sequences, makes it possible to fit both T_1 and T_2 relaxometry signal decays (intensities) at the same time as B_1. We formulate the estimation as a single energy problem depending on four parameters per voxel (T_1, T_2, M_0, B_1) plus one global parameter k over the image. Our approach amounts to minimizing the following energy function over the entire image space V:

$$\mathcal{E} = \lambda E_r(B_1) + \int_V \sum_{i=1}^{2} \left(S_{\alpha_i} - kI_{\alpha_i}(T_1, M_0, B_1)\right)^2 + \sum_{j=1}^{n} \left(S_{\mathrm{TE}_j} - I_{\mathrm{TE}_j}(T_1, T_2, M_0, B_1)\right)^2 \tag{3}$$

where B_1 represents the field inhomogeneities under the assumption that the transmission field is a linear system. The coefficient k is a voxel-independent scale factor, accounting for the global change of M_0 between T_1 and T_2 relaxometry sequences. This assumption of a stationary k factor is reasonable when considering that the time between T_1 and T_2 relaxometry sequences acquisitions is short. There is therefore no large variation arising from transmitter and receiver effects between these two relaxometry sequences and the k values originated from different voxels are approximately constant in the whole brain.

This energy function is made of three terms. The first one in the integral depends on the T_1 relaxometry sequences with a modified signal equation I_{α_i} with α_i accounting for B_1 inhomogeneities. This is done by replacing the flip angles α in T_1 and T_2 relaxometry signals (Sect. 2.1) by $\alpha = B_1\alpha_{\mathrm{nomi}}$ where α_{nomi} is the nominal value of the flip angle. The second term in the integral is related to the T_2 relaxometry sequences. Again, we utilize the EPG expression for the signal equation I_{TE_j} at the j-th echo, with the flip angle α accounting for B_1. Finally, the term E_r introduces an L_2 regularization of the B_1 field to account for the fact that those inhomogeneities vary slowly in space.

2.3 Proposed Algorithm: Parameters Estimation

It is worth noting that the energy function $\mathcal{E}$ is convex with regard to k, M_0 and T_2 respectively. To simplify the optimization process, we estimate the parameters of this function using an alternated minimization process, as follows:

1. Initialize T_1, T_2 and M_0 from regular estimation (Sect. 2.1). B_1 is set to 1.
2. Minimize $\mathcal{E}$ alternately (fixing other parameters) with respect to k, T_2, M_0, B_1 and T_1.
3. Regularize B_1 with a Gaussian kernel.
4. Go to step 2 until convergence has been reached.

Estimating k amounts to solving a least squares problem between T_1 relaxometry signals and the simulated ones from current values of the parameters. However, to account for outliers in the estimation caused by voxels outside of the brain (vessels, bones), we estimate k using Tukey's Bisquare M-estimator [16]. Similarly, M_0 has an analytical solution at each voxel. Estimating the other parameters is more complicated as derivatives are not easily computed. We therefore perform the alternated minimizations using the BOBYQA algorithm for bounded optimization without gradient [11] subject to constraints extracted from the literature: $M_0 \geq 0$, $0 \leq T_1 \leq 5000$ ms, $0 \leq T_2 \leq 1000$ ms and $0.2 \leq B_1 \leq 2$ [6, 13, 5]. We regularize B_1 as a separate smoothing step to account for the B_1 inhomogeneities in space.

3 Experimental Design for Validation

The validation process included synthetic phantom and in vivo measurements. Both synthetic phantom and in vivo tests used the following parameters to simulate/acquire the relaxometry sequences: (1) for the T_1 relaxometry: voxel size: $1.3 \times 1.3 \times 3$ mm^3, TR = 15 ms, TE = 1.54 ms, FA: 5° and 30°; (2) for the T_2 relaxometry: voxel size: $1.3 \times 1.3 \times 3$ mm^3, TR = 4530 ms, TE = $[13.8, 27.6, 41.4, 55.2, 69.0, 82.8, 96.6]$ ms.

3.1 Synthetic Phantom

We generated a synthetic phantom to quantitatively evaluate the results of T_1 and T_2 estimations. The phantom was made of three types of tissues organized in concentric spheres, which are cerebrospinal fluid (CSF), white matter (WM), and gray matter (GM). All reference values are taken as similar to values in the human brain[1] (Tab. 1). To demonstrate the capability to retrieve realistic B_1 maps, B_1 was set to different values: smaller than 1 for GM and higher than 1 for CSF and WM. Since B_1 is generally high at the center of the scene [5], we set B_1 for CSF to be the largest among all tissues. The reference value of k is set to be 7. The reference relaxation maps (see Fig. 1) were used to feed

[1] The T_1, T_2 and M_0 values are given by `http://www.bic.mni.mcgill.ca/brainweb/`

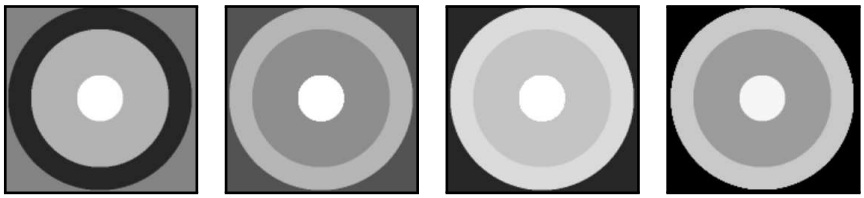

Fig. 1. The synthetic phantom. From left to right: B_1, T_1, T_2 and M_0 reference maps.

into an MRI simulator[2] in order to synthesize T_1 and T_2 relaxometry sequences following signal equations from Sect. 2.1 with α accounting for B_1. Then we added Rician noise to the simulated relaxometry sequences (SNR= 20dB). The estimation was run with the regular DESPOT1 and EPG estimations (Sect. 2.1) and with the proposed method. The results were then compared to the reference values to quantitatively evaluate our algorithm.

3.2 In Vivo Study

In vivo validation was performed on a high field MRI scanner (3T Siemens Verio VB17), which has significant effects of B_1 field inhomogeneities. Whole-brain MR images were acquired on 13 healthy subjects (6 male, 7 female, mean age= 29.2 ± 17.8 y.o.). To compensate for between-scans subject motion, a six-parameter rigid-body registration was carried out for each subject based on normalized mutual information. We acquired T1-w SE and T2-w/PD-w MR sequences for each subject and considered these real acquisitions as references for in vivo validation. Then the estimated maps (with our method and with the methods described in Sect. 2.1) were used to feed into the MRI simulator[2] to generate T1-w, T2-w and PD-w images with the same sequences and parameters as the real acquisitions. Note that for all simulations, we applied bias field correction of the M_0 map as it is sensitive to the coil sensitivity. This correction is based on a unified segmentation [1]. To quantitatively evaluate the performance of the algorithms, we use the squared correlation coefficient R, computed between the real and the simulated images, as an indicator of the estimation accuracy. Assuming the simulations are perfect, the closer the R values are to 1, the better the map estimations.

4 Results

4.1 Synthetic Phantom

We present in Tab. 1 the comparison between the reference and estimated values for T_1, T_2, B_1 and M_0 using the two evaluated methods. It can be seen that the DESPOT1 algorithm is sensitive to B_1 inhomogeneities due to its inability to

[2] SimuBloch v0.3 at `http://vip.creatis.insa-lyon.fr`

estimate those values. The estimated T_1 and M_0 therefore vary significantly from the reference values. However, when we applied the proposed algorithm, the estimated B_1, T_1, T_2 and M_0 are in close agreement with the reference values. The reference values are always included within one standard deviation of the estimated values using the proposed method.

Tissue	Method	Ave(B_1)	Std(B_1)	Ave(T_1)	Std(T_1)	Ave(T_2)	Std(T_2)	Ave(M_0)	Std(M_0)
WM	Reference	1.10	0.00	500.00	0.00	70.00	0.00	80.00	0.00
	Regular	–	–	608.06	0.71	71.31	1.97	77.55	1.59
	Proposed	**1.10**	0.00	**495.97**	15.71	**69.84**	1.69	**80.32**	1.13
GM	Reference	0.80	0.00	830.00	0.00	80.00	0.00	90.00	0.00
	Regular	–	–	526.88	0.87	87.26	2.47	79.10	1.47
	Proposed	**0.80**	0.00	**823.50**	60.30	**79.91**	2.57	**90.22**	3.12
CSF	Reference	1.30	0.00	2500.00	0.00	330.00	0.00	100.00	0.00
	Regular	–	–	4364.33	449.69	476.14	48.61	75.95	1.12
	Proposed	**1.30**	0.00	**2485.96**	193.76	**329.73**	27.13	**100.50**	3.33

Table 1. Statistical values of B_1, T_1 (ms), T_2 (ms) and M_0 on the synthetic phantom. Ave and Std are the mean and standard deviation. The estimated k is 6.94.

4.2 In Vivo Results

Fig. 2 presents the maps estimated using the regular method and the proposed algorithm. This figure confirms visually that the regular algorithm is sensitive to B_1 inhomogeneities, especially seen on T_1 maps where the center values are much higher for the same tissues. On the contrary, the proposed method removes the influence of B_1 inhomogeneities and the obtained maps are much more uniform.

Fig. 3 presents the T1-w images from the real acquisition and from the simulation using the regular method and the proposed algorithm. The results of T2-w and PD-w simulations were computed for quantitative evaluation but are not presented as all simulations look very similar to the real acquisitions. On this figure, it is clear that the regular method's inability to estimate B_1 results in degraded simulations for T1-w sequences. These observations are confirmed by the R coefficients in Tab. 2. All values are significantly increased (paired t-test, $p < 10^{-6}$ for each of the simulated sequences) between the regular and proposed methods. Moreover, the correlation coefficients for T1-w images increase over 50% using the proposed method (0.653 compared to 0.327).

5 Conclusion

We have proposed a new approach for simultaneous mapping of B_1 inhomogeneity field, T_1 and T_2 relaxation times, and proton density M_0. The method is based on the intrinsic correlation between the T_1 and T_2 relaxometry sequences. We use a combined model of DESPOT1 and EPG algorithms to estimate T_1, T_2, M_0 and

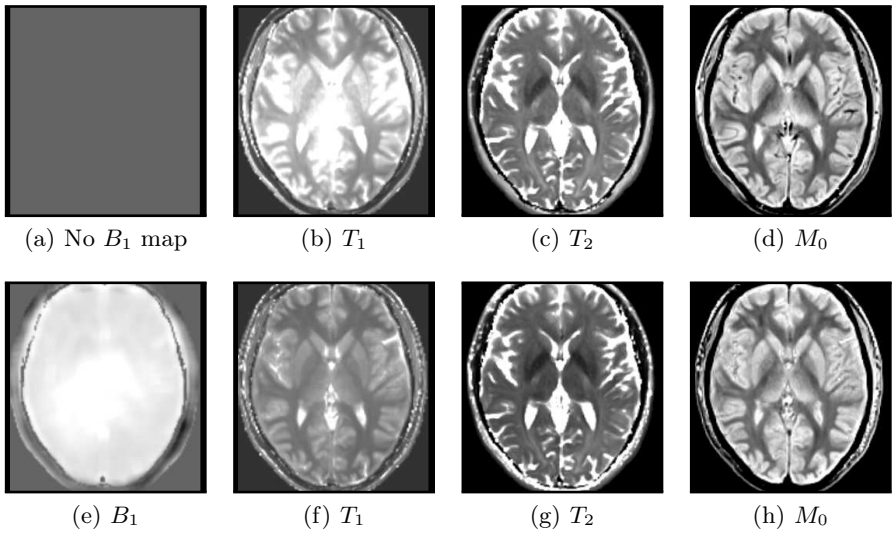

(a) No B_1 map (b) T_1 (c) T_2 (d) M_0

(e) B_1 (f) T_1 (g) T_2 (h) M_0

Fig. 2. Estimated maps on one healthy subject. Row 1 shows the maps using the regular method, row 2 using the proposed method. From left to right for each row: B_1, T_1, T_2 and M_0 maps respectively. The same window level is set for each column.

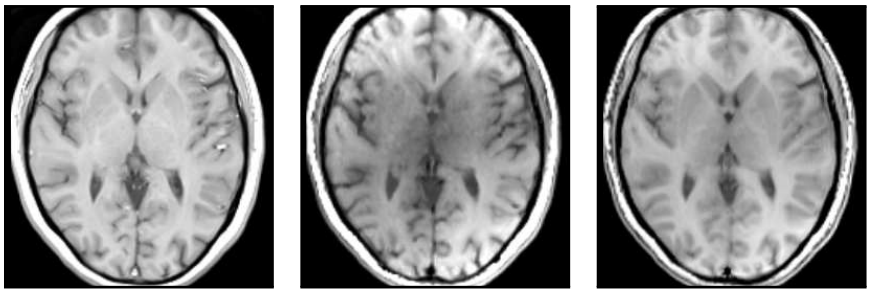

Fig. 3. Simulated T1-w images and the corresponding real acquisition on one healthy subject. From left to right: real acquisition, simulated images using the regular and the proposed methods respectively.

	T1-w Ave(R)	T1-w Std(R)	T2-w Ave(R)	T2-w Std(R)	PD-w Ave(R)	PD-w Std(R)
Regular	0.327	0.092	0.894	0.018	0.729	0.051
Proposed	0.653	0.107	0.923	0.016	0.834	0.026

Table 2. Average correlation coefficient R between the simulated images and the real acquisitions on 13 healthy subjects, for T1-w, T2-w and PD-w images. Row 1 shows R for the regular method, row 2 for the proposed algorithm. Differences are significant (paired t-test, $p < 10^{-6}$).

B_1 simultaneously. This combination requires no additional sequence for the B_1 correction, making use of the traditional T_1 and T_2 relaxometry sequences only.

Our experiments on simulated data demonstrated that the proposed method is able to accurately estimate T_1, T_2, M_0 and B_1 maps. Experiments on in vivo data showed high correlation (up to 50 % increase) between the weighted acquisitions and the simulated sequences, which confirms the great potential of the proposed method to handle clinical applications where quantitative MRI has been shown to be highly relevant (MS, stroke, pediatrics, ...).

References

1. Ashburner, J., Friston, K.: Unified segmentation. NeuroImage 26, 839–851 (2005)
2. Collins, C.M., Li, S., Smith, M.B.: SAR and B1 field distributions in a heterogeneous human head model within a birdcage coil. MRM 40(6), 847–56 (1998)
3. Deoni, S.: High-resolution T1 mapping of the brain at 3T with driven equilibrium single pulse observation of T1 with high-speed incorporation of RF field inhomogeneities (DESPOT1-HIFI). J Magn Reson Imaging 26(4), 1106–11 (2007)
4. Deoni, S., Rutt, B., Peters, T.: Rapid combined T1 and T2 mapping using gradient recalled acquisition in the steady state. MRM 49(3), 515–526 (2003)
5. Dowell, N.G., Tofts, P.S.: Fast, accurate, and precise mapping of the RF field in vivo using the 180 degrees signal null. Magn Reson Med 58(3), 622–30 (2007)
6. Gelman, N., Gorell, J., Barker, P., Savage, R., Spickler, E., Windham, J., Knight, R.: MR imaging of human brain at 3T: preliminary report on transverse relaxation rates and relation to estimated iron content. Radiology 210(3), 759–767 (1999)
7. Hennig, J.: Multiecho imaging sequences with low refocusing flip angles. Journal of Magnetic Resonance (1969) 78(3), 397–407 (Jul 1988)
8. Layton, K., Morelande, M., Wright, D., Farrell, P., Moran, B., Johnston, L.: Modelling and estimation of multicomponent T_2 distributions. IEEE TMI 32(8), 1423–1434 (2013)
9. Lebel, R.M., Wilman, A.H.: Transverse relaxometry with stimulated echo compensation. Magn. Reson. Med. 64(4), 1005–1014 (2010)
10. Parker, G.J.M., Barker, G.J., Tofts, P.S.: Accurate multislice gradient echo T_1 measurement in the presence of non-ideal RF pulse shape and RF field nonuniformity. Magnetic Resonance in Medicine 45(5), 838–845 (2001)
11. Powell, M.: The BOBYQA algorithm for bound constrained optimization without derivatives. Tech. rep., Centre for Mathematical Sciences, University of Cambridge, UK (2009)
12. Prasloski, T., Mädler, B., Xiang, Q.S.S., MacKay, A., Jones, C.: Applications of stimulated echo correction to multicomponent T2 analysis. Magnetic resonance in medicine 67(6), 1803–1814 (Jun 2012)
13. Stanisz, G., Odrobina, E., Pun, J., Escaravage, M., Graham, S., Bronskill, M., Henkelman, R.: T1, T2 relaxation and magnetization transfer in tissue at 3T. MRM 54(3), 507–512 (2005)
14. Tofts, P.: Quantitative MRI of the Brain: Measuring Changes Caused by Disease. John Wiley & Sons, Ltd (2003)
15. Treier, R., Steingoetter, A., Fried, M., Schwizer, W., Boesiger, P.: Optimized and combined T1 and B1 mapping technique for fast and accurate T1 quantification in contrast-enhanced abdominal MRI. Magn Reson Med 57(3), 568–76 (2007)
16. Tukey, J.: Exploratory Data Analysis. Addison-Wesley Publishers, Cy (1977)
17. Yarnykh, V.L.: Actual flip-angle imaging in the pulsed steady state: A method for rapid three-dimensional mapping of the transmitted radiofrequency field. Magn. Reson. Med. 57(1), 192–200 (Jan 2007)